

**Reduced diffusion in normal appearing white matter of glioma patients following radio(chemo)therapy**

Raschke, F.; Wesemann, T.; Wahl, H.; Appold, S.; Krause, M.; Linn, J.; Troost, E. G. C.;

Originally published:

June 2019

**Radiotherapy and Oncology 140(2019), 110-115**

DOI: <https://doi.org/10.1016/j.radonc.2019.06.022>

Perma-Link to Publication Repository of HZDR:

<https://www.hzdr.de/publications/Publ-29101>

Release of the secondary publication  
on the basis of the German Copyright Law § 38 Section 4.

CC BY-NC-ND

# Reduced diffusion in normal appearing white matter of glioma patients following radio(chemo)therapy

**F. Raschke<sup>1,2,3\*</sup>, T. Wesemann<sup>4</sup>, H. Wahl<sup>4</sup>, S. Appold<sup>2,5</sup>, M. Krause<sup>1,2,3,5,6</sup>, J. Linn<sup>4</sup>, E.G.C. Troost<sup>1,2,3,5,6</sup>**

<sup>1</sup> Institute of Radiooncology - OncoRay, Helmholtz-Zentrum Dresden-Rossendorf, Rossendorf, Germany;

<sup>2</sup> OncoRay - National Center for Radiation Research in Oncology, Faculty of Medicine and University Hospital Carl Gustav Carus, Technische Universität Dresden, Helmholtz-Zentrum Dresden – Rossendorf, Dresden, Germany;

<sup>3</sup> National Center for Tumor Diseases (NCT), Partner Site Dresden, Germany: German Cancer Research Center (DKFZ), Heidelberg, Germany; Faculty of Medicine and University Hospital Carl Gustav Carus, Technische Universität Dresden, Dresden, Germany, and; Helmholtz Association / Helmholtz-Zentrum Dresden - Rossendorf (HZDR), Dresden, Germany;

<sup>4</sup> Institute of Neuroradiology, University Hospital Carl Gustav Carus and Medical Faculty of Technische Universität, Dresden, Germany;

<sup>5</sup> Department of Radiotherapy and Radiation Oncology, Faculty of Medicine and University Hospital Carl Gustav Carus, Technische Universität Dresden, Dresden, Germany;

<sup>6</sup> German Cancer Consortium (DKTK), Partner Site Dresden, and German Cancer Research Center (DKFZ), Heidelberg, Germany;

\*Author for correspondence – Felix Raschke, [felix.raschke@oncoray.de](mailto:felix.raschke@oncoray.de), +49 351 458 6538, OncoRay, Medizinische Fakultät, PF41, Fetscherstr. 74, 01307 Dresden, Germany

Keywords: White Matter; Grey Matter; Diffusion Tensor Imaging; Radiotherapy; quantitative MRI; Proton Therapy; Photon Therapy; glioma; normal tissue

## Abstract

### *Background and purpose:*

Standard treatment of high grade gliomas includes gross tumour resection followed by radio(chemo)therapy. Radiotherapy inevitably leads to irradiation of normal brain tissue. The goal of this prospective, longitudinal study was to use MRI to quantify normal appearing white and grey matter changes following radiation treatment as a function of dose and time after radiotherapy.

### *Materials and methods:*

Pre-radiotherapy MRI (proton or photon therapy) and follow-up MRIs collected in 3 monthly intervals thereafter were analysed for 22 glioma patients and included diffusion tensor imaging, quantitative T1, T2\* and proton density mapping. Abnormal tissue was excluded from analysis. MR signal changes were quantified within different dose bin regions for grey and white matter and subsequently for whole brain white matter.

### *Results:*

We found significant reductions of mean diffusivity, radial diffusivity, axial diffusivity and T2\* in normal appearing white matter regions receiving a radiation dose as low as 10-20 Gy within the observational period of up to 18 months. The magnitude of these changes increased with the received radiation dose and progressed with time after radiotherapy. Whole brain white matter also showed a significant reduction in radial diffusivity as a function of radiation dose and time after radiotherapy. No significant changes were observed in grey matter.

### *Conclusion:*

Diffusion tensor imaging and T2\* imaging revealed normal appearing white matter changes following radiation treatment. The changes were dose dependant and progressed over time. Further work is needed to understand the underlying tissue changes and to correlate the observed diffusion changes with late brain malfunctions.

## Abbreviations

|      |   |  |
|------|---|--|
| T1w  | - | T1-weighted                                |
| T2w  | - | T2-weighted                                |
| AD   | - | axial diffusivity                          |
| CT   | - | computed tomography                        |
| CSF  | - | cerebrospinal fluid                        |
| CTV  | - | clinical target volume                     |
| DTI  | - | diffusion tensor imaging                   |
| FA3  | - | 3D gradient echo image with flip angle 3°  |
| FA20 | - | 3D gradient echo image with flip angle 20° |
| FA   | - | fractional anisotropy                      |
| GM   | - | grey matter                                |
| GTV  | - | gross tumour volume                        |
| HC   | - | healthy control                            |
| MD   | - | mean diffusivity                           |
| PD   | - | proton density                             |
| PTV  | - | planning target volume                     |
| RD   | - | radial diffusivity                         |
| RTx  | - | radiotherapy                               |
| SDAM | - | saturated double angle method              |
| TBV  | - | termed tumour bed volume                   |
| WM   | - | white matter                               |

## 1. Introduction

Gliomas are the most common primary brain tumour in adults. Standard treatment of high grade gliomas includes gross tumour resection followed by radiotherapy with simultaneous or subsequent chemotherapy. The clinical target volume used for radiotherapy typically includes the resection cavity, the area of contrast enhancement seen on T1-weighted (T1w) MRI with an additional margin of 1 - 3 cm and T2-weighted (T2w) hyperintense areas to irradiate potential tumour infiltration [1, 2]. Consequently, this leads to large irradiated volumes which inevitably include normal brain tissue. This can induce radiation related brain injuries which comprise anatomical changes, such as oedema, demyelination, gliosis and vascular abnormalities, as well as functional deficits, including short-term memory loss and cognitive impairment [3].

Irradiation with protons instead of photons reduces the radiation dose to surrounding brain in glioma patients [4]. To investigate if this reduction in radiation dose to normal appearing brain translates to measurable benefits for the patients, prospective clinical trials are ongoing, assessing the quality of life, neurocognitive functioning and MR image changes. In previous studies, radiation-induced normal tissue damage was assessed using oedema, haemorrhage or necrosis scored as binary events on T2w and contrast enhanced T1w MRI [5-7]. Drawbacks of these approaches are the loss of spatial information and low incidence rates [5, 8], resulting in low predictive values. Additionally, there is a variable latency between irradiation and the occurrence of such severe side-effects. An early biomarker of late brain malfunctions or neurocognitive impairments would largely improve clinical trials and would enhance their capability to assess normal tissue complication rates in brain tumour radiotherapy.

Diffusion tensor imaging (DTI) allows probing of the tissue microstructure and therefore holds potential to detect earlier and less severe tissue changes not visible on conventional anatomical MRI. DTI has also proven to be a robust technique with low variability in a multicentre setting [9]. The most commonly used DTI parameters are fractional anisotropy (FA), mean diffusivity (MD), radial diffusivity (RD) and axial diffusivity (AD). Previous studies investigated primarily white matter (WM) diffusion changes following radiotherapy either within the whole brain [10, 11] or focused on specific regions or tracts [12-19]. The most common diffusion results were a decrease in FA [10, 12, 14, 15, 19] and increased RD [10-12, 14-16, 19] consistent with demyelination [20, 21], although deviations from this pattern were also reported [17, 18].

Other relevant quantitative MR measures include T1, proton density (PD) and T2\*. T1 has shown to be a sensitive marker for myelin [22] and thus has the potential to support diffusion results related to

demyelination or axonal loss. Similarly, quantitative PD mapping can be used to control for build-up or resolving of oedema, whereas T2\* is used to assess tissue heterogeneity.

The aim of this longitudinal, prospective study was to quantify radiation-induced normal appearing brain changes as function of radiation dose and time after radio(chemo)therapy. For this, we measured DTI as well as quantitative T1, PD and T2\* changes within the normal appearing brain in a cohort of glioma patients. To minimize the impact of potential tumour progress on our analysis, we exclude all abnormal tissue across all time points from the analysis to solely focus on normal appearing white matter and grey matter (GM). Given the previously reported results, we hypothesized that FA and T1 decrease and RD increases in white matter, consistent with demyelination. We expected these changes to progress over time and to increase in magnitude with the received radiation dose.

## 2. Methods

### Subjects

Data from glioma patients was taken from an ongoing, longitudinal study, which was approved by the local ethics committee [NCT02824731, EK22012016]. All patients underwent primary gross tumour resection followed by radio(chemo)therapy. Of 40 recruited patients, 27 patients had a pre-radiotherapy multimodal MRI and at least one identical follow-up MRI available. Follow-up scans were performed approximately 3 months after the end of radiotherapy and in 3-monthly intervals thereafter. Time points corresponding to histologically confirmed tumour progression were excluded, leaving data from 22 patients (age  $47.8y \pm 13.9y$ , range [28.9y – 76.7y], 9 male) available for analysis. Clinical details and individual exclusion criteria for individual time points are listed in supplementary Table 1.

Additionally, six healthy controls (HCs) (age  $39.4y \pm 8.7y$ , range [30.6y – 54.2y], 4 male) underwent two multimodal MRI scans with an interval of  $3.6 \pm 0.5$  months. This study was approved by the local ethics committee, and the participants gave written informed consent [DRKS-ID: DRKS00012600, EK267072017]. The healthy control MR data was collected in parallel to the patient data using the identical set-up described in the following section.

### Data acquisition

All MRI data were acquired on a 3T Philips Ingenuity PET/MR scanner (Philips, Eindhoven, The Netherlands) using an 8 channel head coil.

DTI data was acquired with TR=6500 ms, TE=66 ms, FOV  $224 \times 224$  mm<sup>2</sup>, matrix size  $112 \times 112$ , slice thickness 2 mm, 60 slices, SENSE(AP)=2, 32 diffusion directions at  $b=1000$  s/mm<sup>2</sup> and two  $b=0$  s/mm<sup>2</sup> volumes without diffusion gradients. Two additional  $b=0$  s/mm<sup>2</sup> volumes were acquired at identical parameters with opposite phase encoding direction.

3D FLAIR images were acquired in sagittal orientation with FOV  $250 \times 250$  mm<sup>2</sup>, acquisition matrix  $252 \times 249$ , reconstruction matrix  $512 \times 512$ , reconstructed slice thickness of 0.5 mm using overcontiguous slices, 360 slices, TR=4800 ms, TE=293 ms, TI=1650 ms, 2 averages.

For T1 and PD mapping, two 3D gradient spoiled echo volumes were acquired in sagittal orientation with flip angles 3° (FA3) and 20° (FA20), TR=10 ms, TE=3.7 ms, FOV  $224 \times 224$ , matrix size  $224 \times 224$ , 1 mm slice thickness, 160 slices and Philips default RF-phase increment of 150°. For T2\* mapping, axial 2D FFE images were acquired with TR=1355 ms, TE<sub>s</sub>=5.8/9.1/12.4/15.8/19.1 ms, FOV  $256 \times 256$  mm<sup>2</sup>,

acquisition matrix 128×128, 47 slices with 2 mm thickness and 1 mm gap. A B1 map was acquired using the saturated double angle method (SDAM) [23] with flip angles 60° & 120°, TR=734 ms, TE=113 ms, FOV 224×224, matrix size 64×64, 4 mm slice thickness and 35 axial slices.

### **Radiation treatment planning**

Computed tomography (CT) scans for radiation treatment planning were performed prior to radio(chemo)therapy with the patient positioned supine with an individual head support and mask. For radiation treatment planning, the CTs were co-registered with the pre- and post-surgery MRI scans (T1w, T2w, T1w with intravenous contrast agent) to define the tumour bed and potential residual tumour (termed tumour bed volume; TBV, or gross tumour volume; GTV, respectively). Depending on the tumour histology, the GTV/TBV was expanded by a 1-2 cm isotropic margin, corrected for anatomical boundaries, to derive the clinical target volume (CTV). For proton therapy, dose was prescribed to the CTV taking into account inherent proton range uncertainties, whereas for photon beam irradiation, a planning target volume (PTV) was computed expanding the CTV by an isotropic margin of 0.5 cm. For this analysis, the planning CTs, corresponding dose maps and CTV contours were retrieved from the planning workstation. CTV contours were converted to binary masks.

### **Data processing**

In this study we focus on the analysis of normal appearing grey and white matter. Consequently, abnormality ROIs covering resection cavities and surrounding abnormal tissue were manually contoured on reconstructed axial FLAIR images with 4 mm slice thickness for each patient and each visit to exclude these areas from further analysis.

DTI data was processed with topup [24] implemented in FSL [25] to correct for geometric distortions caused by B0 inhomogeneities and FSL dtifit to estimate the diffusion tensor for each voxel. Subsequently, maps for FA, MD, AD, RD and  $q$  maps were calculated. The anisotropy measure  $q$  was previously proposed and unlike FA is not normalised by the root mean square diffusion [26].

T2\* maps were calculated from the 2D FFE images on the scanner console, assuming a mono-exponential decay. Quantitative T1 and PD maps were calculated from the FA3 and FA20 images and using the B1 and T2\* maps. The resulting T1 maps were segmented into GM, WM and CSF using SPM12 (Statistical Parametric Mapping: <https://www.fil.ion.ucl.ac.uk/spm/>) after manually excluding all abnormal tissue using the previously created abnormality ROIs. These GM and WM masks were transferred to DTI and T2\* space via a rigid body registration using ANTs [27, 28].

Detailed data processing steps are described in the supplementary materials.



## Data analysis

All analyses focused on whole brain normal appearing white matter and grey matter. Normal appearing brain was defined as being outside the CTV and the previously drawn abnormality ROI. To ensure exclusion of the same tissue areas across all relevant time points, a combined abnormality mask across all visits was created for each patient. This was done by warping each abnormality mask to MNI space via the T1w images and warping the combined masks back to the original T1w images using ANTs [27, 28](see supplementary Figure 1). The cerebellum and brain stem were excluded from all analyses due to varying spatial coverage by the MRI sequences. This was done by warping the MNI standard brain and a corresponding cerebrum mask to each T1w image of each patient and each visit (see supplementary Figure 4).

In the first analysis, whole brain MR signal changes were calculated within different dose regions across all time points. For this, dose maps were divided into seven dose bins: 0-3 Gy, 3-10 Gy, 10-20 Gy, 20-30 Gy, 30-40 Gy, 40-50 Gy, >50Gy. Mean signal intensities were extracted from whole brain GM (T2\*, MD, T1, PD) and whole brain WM (T2\*, T1, PD, MD, FA, q, AD, RD) for each dose bin using a tissue probability threshold of 0.95. Only voxels outside the CTV and combined abnormality ROI were considered. Dose bin regions containing less than 100 voxels were excluded from the analysis. A relative signal change between follow-up and baseline values was calculated as  $\Delta S[\%]=100\times(S_f - S_{base})/S_{base}$ . The mean relative signal change was calculated across all patients and for each dose bin region, and reported in the results section. The HC data set served as a control cohort to reveal potential systematic errors. We therefore warped the dose maps, CTV masks and combined abnormality masks from 22 patients to each of the six HC data sets via MNI space using ANTs (see supplementary Figure 5A & 5B), resulting in a total of  $6\times 22=132$  permutations. Similar to the patient data, the mean relative signal change across all 132 permutations was calculated for all dose bin regions. Relative signal changes in both the patient data and HC control data were evaluated using paired t-tests. A Bonferroni correction factor for multiple comparisons of 12 (4 comparisons in GM and 8 comparisons in WM) was used, resulting in a significance threshold of 0.0042.

In a second analysis, we investigated the impact of both time after radiotherapy and mean dose on whole brain white matter T2\* and RD changes. For this, the mean MR signal and mean radiation dose were determined across all normal appearing WM voxels. The relative signal change  $\Delta S$  was calculated for T2\* and RD and across all available time points. A mixed linear model with repeated measurements  $\Delta S[\%]=b_0+b_1\times Dose[Gy]+b_2\times Time[months]$  was used to assess the influence of both time and mean dose on whole white matter T2\* and RD changes, respectively (SPSS, IBM Corp. Released 2017. IBM SPSS Statistics for Windows, Version 25.0. Armonk, NY: IBM Corp.).



### 3. Results

Imaging data at 3, 6, 9, 12, 15 and 18 months after radio(chemo)therapy was available for  $N = 19, 15, 12, 11, 6$  and  $5$  patients, respectively. Figure 1 shows a complete set of quantitative axial images and corresponding grey matter and white matter masks for one patient.

Figure 2 shows the mean relative MD, AD, RD, FA and  $T2^*$  changes within the different dose bins in white matter. MD, AD, RD and  $T2^*$  were significantly reduced both over time and dose, whereas the diffusion changes preceded  $T2^*$  changes. FA showed a significant increase at high doses, whereas the anisotropy measure  $q$  showed no dose dependent changes (supplementary Figure 7). Albeit there was a small, but significant reduction in  $q$  three months after radio(chemo)therapy, which normalised in the later time points. Neither T1 nor PD showed any significant changes (supplementary Figure 7). No significant changes were observed in grey matter (supplementary Figure 8). In the untreated control cohort, there were some systematic offsets smaller than 2% (see Figure 2, supplementary Figure 7 and supplementary Figure 8), however, no dose dependent changes were observed in either grey or white matter.

Following these results, we used a mixed linear model to investigate the influence of both time after radiotherapy and mean dose on whole brain white matter  $T2^*$  and RD changes, respectively. We chose these two parameters, since they showed the largest magnitude of relative signal changes in the dose bin analysis. Mean dose in normal appearing white matter was  $13.6 \pm 9.7$  Gy (protons:  $9.6 \pm 4.6$  Gy,  $N=17$ ; photons  $29.9 \pm 10.2$  Gy,  $N=4$ ; one patient with mixed treatment). The results of the linear mixed models for RD and  $T2^*$  are shown in Table 1. RD significantly reduced with both mean dose and time at rates of  $-0.15$  % per Gy ( $p=0.003$ ) and  $-0.18$  % per month ( $p<0.001$ ), respectively.  $T2^*$  changes were only significantly associated with time at  $-0.13\%$  per month ( $p=0.002$ ), but not with the mean dose ( $p=0.177$ ). An animation of the mixed linear model fitted to the RD changes observed in white matter can be found in the supplementary material.

## 4. Discussion

We hypothesised that, following radiation, FA would decrease and RD would increase with time and dose in normal appearing white matter thus mimicking typical diffusion observations associated with demyelination and axonal loss. Instead, we observed dose dependent and time progressive reductions of RD, MD, AD and T2\*. Additionally we have seen a trend of increasing FA, which is likely driven by the reduction of MD rather than a real anisotropy increase in the white matter. This is supported by the fact that the anisotropy measure  $q$  did not increase [26]. We therefore do not observe expected signs of axonal demyelination within our data, which is supported by stable T1 values, a sensitive marker for myelin [22]. Additionally, it has been shown that demyelinated white matter in mice shows significantly increased T2\* [29], whereas we observe a significant T2\* decrease.

The MD reduction in white matter following radiotherapy is mainly driven by a reduction in RD. A decrease of RD in white matter is usually associated with axonal swelling, as observed in acute and early phases of stroke [30]. Although in our study the RD decrease was in the order of 10%, compared to well over 50% in stroke and therefore not easily assessed visually.

Most previous studies investigating diffusion changes in white matter following radiotherapy found a decrease in FA and increase in MD and RD ranging from 2%-50%, which is commonly interpreted as demyelination or axonal damage [10, 12, 14, 16]. For AD, both increase [10-12] and decrease was previously reported [14, 16, 18]. Using tract-based spatial statistics (TBSS), Connor et al. [17] found patterns of FA decrease and RD and AD increase. However, they equally found white matter bundles with opposite behaviour, showing a significant AD and RD decrease. In a separate study, Zhu et al. [18] measured a significant decrease of AD and RD in white matter fibres after radiotherapy. Reactive astrogliosis, axonal degradation, axonal swelling and resolving oedema were previously suggested as possible explanations for decreasing RD and AD. Resolving oedema can be ruled out as a cause for reduced diffusivity observed in our study, as PD values show no significant changes. Astrogliosis is thought to be a response to cerebral injury but has shown to increase RD and reduce FA in white matter in mice, whereas an FA increase due to astrogliosis was only observed in grey matter [31]. Axonal degradation is a complex process, which includes axonal swelling, glial activation and axonal fragmentation [32]. Observing this process at different stages could explain the diverse diffusion results seen in different studies. Early stages with axonal swelling would cause a diffusion decrease as seen in our results whereas further progression including axonal demyelination is more likely to cause a diffusion increase, similar to the time course seen in stroke [30].

We also observed a significant decrease in  $T2^*$ , which could be caused by increased tissue heterogeneity. This can be an indicator for microglial activation caused by radiation [20, 33] and could therefore also explain the reduction in overall diffusivity due to higher number of cell bodies in the white matter. However, we would then expect to see a simultaneous drop in anisotropy measures, which we did not observe. Additionally, the diffusion changes precede the  $T2^*$  decrease, which might suggest a less direct relationship. The  $T2^*$  reduction could also point towards changes in tissue oxygenation [34] and thus vascular alterations. This is supported by previously reported perfusion reductions observed in grey matter following radiotherapy [35] and would support the ischemia like behaviour of the diffusion metrics, albeit at a much smaller scale.

Future work is needed to connect the observations of this study to the underlying tissue changes. Specifically, we will analyse perfusion changes in white matter following radiotherapy to investigate vascular alterations. Similarly, glial cell density, neuronal health and neuro inflammation will be studied using MR spectroscopy [36]. Additionally, the observation period of the patients needs to be extended to investigate potential recovery of signal intensities and correlate the observed diffusion changes with late brain malfunctions. In a next step, we will investigate if occurrence of FLAIR hyperintensities can be predicted by diffusion reductions from previous time points.

For a more in-depth comparison of proton vs. photon based radiotherapy, a larger data set is needed. This includes investigating the effect of an equivalent proton and photon radiation dose on tissue. Nonetheless, we have shown that mean RD reduces significantly as a function of radiation dose across whole brain white matter. Consequently, these mean white matter changes are smaller in patients treated with protons compared to photons, since these patients typically receive a lower dose to the normal appearing brain.

## Conclusion

We measured significant reductions of MD, AD, RD and  $T2^*$  in white matter of glioma patients following radiotherapy. The magnitude of these changes progressed over time after radiotherapy and was greater in areas that received a higher radiation dose. The largest magnitude in change was observed for RD which also translated to significant time and dose dependant mean RD reductions across whole brain white matter. Further work is needed to understand the underlying tissue changes.

## Acknowledgements

We thank all patients and healthy volunteers for participating in the respective studies. We thank Prof F. A. Howe for the helpful discussions and both A. Dutz and Dr. S. Löck for advice on statistical analysis. This work was partly funded by the National Center for Tumor Diseases (NCT), Partner Site Dresden.

## Figures

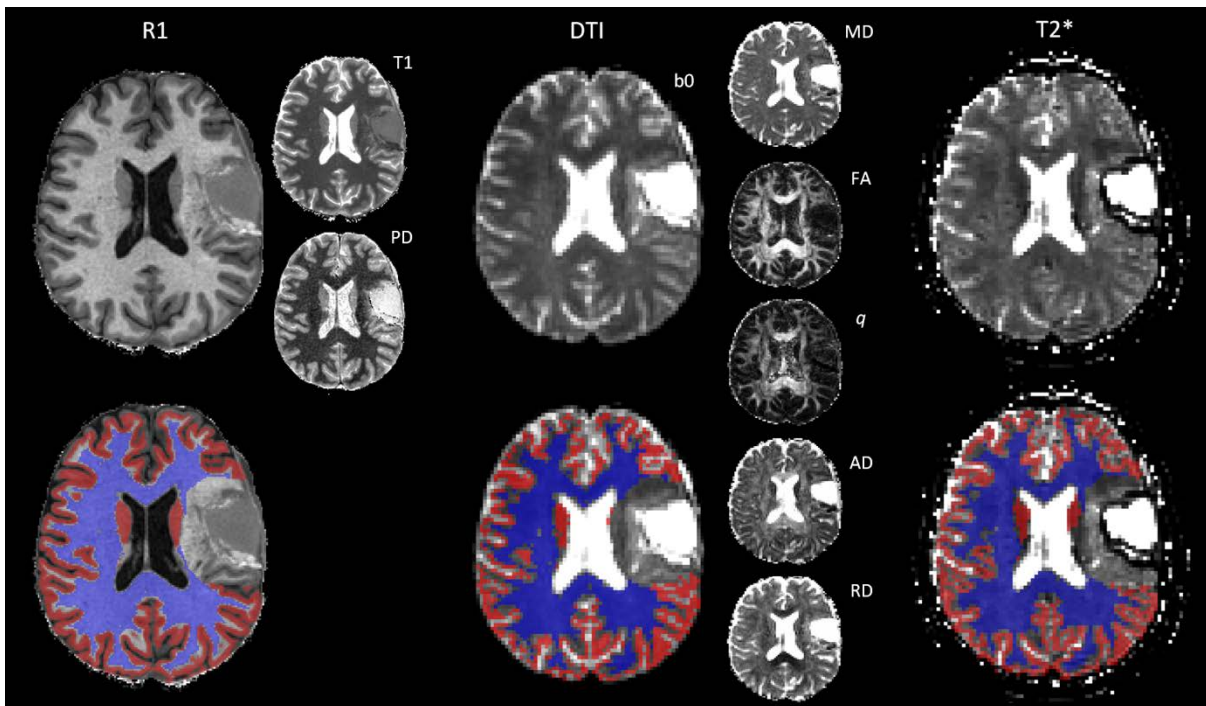


Figure 1: Overview of the multiparametric MR images of a patient (#9) with a resected grade III anaplastic astrocytoma before the start of radiotherapy and adjuvant chemotherapy [PCV: consisting of procarbazine, lomustine (CCNU) and vincristine]. GM and WM masks were obtained by SPM12 segmentation of the T1 map. The GM (red) and WM masks (blue) were coregistered to the DTI b0 image and T2\* map using a rigid body transformation and nearest neighbour interpolation. A subsequent probability threshold of 0.95 was chosen to binarize the GM and WM maps. Abnormal tissue was masked out prior to segmentation.

5

10

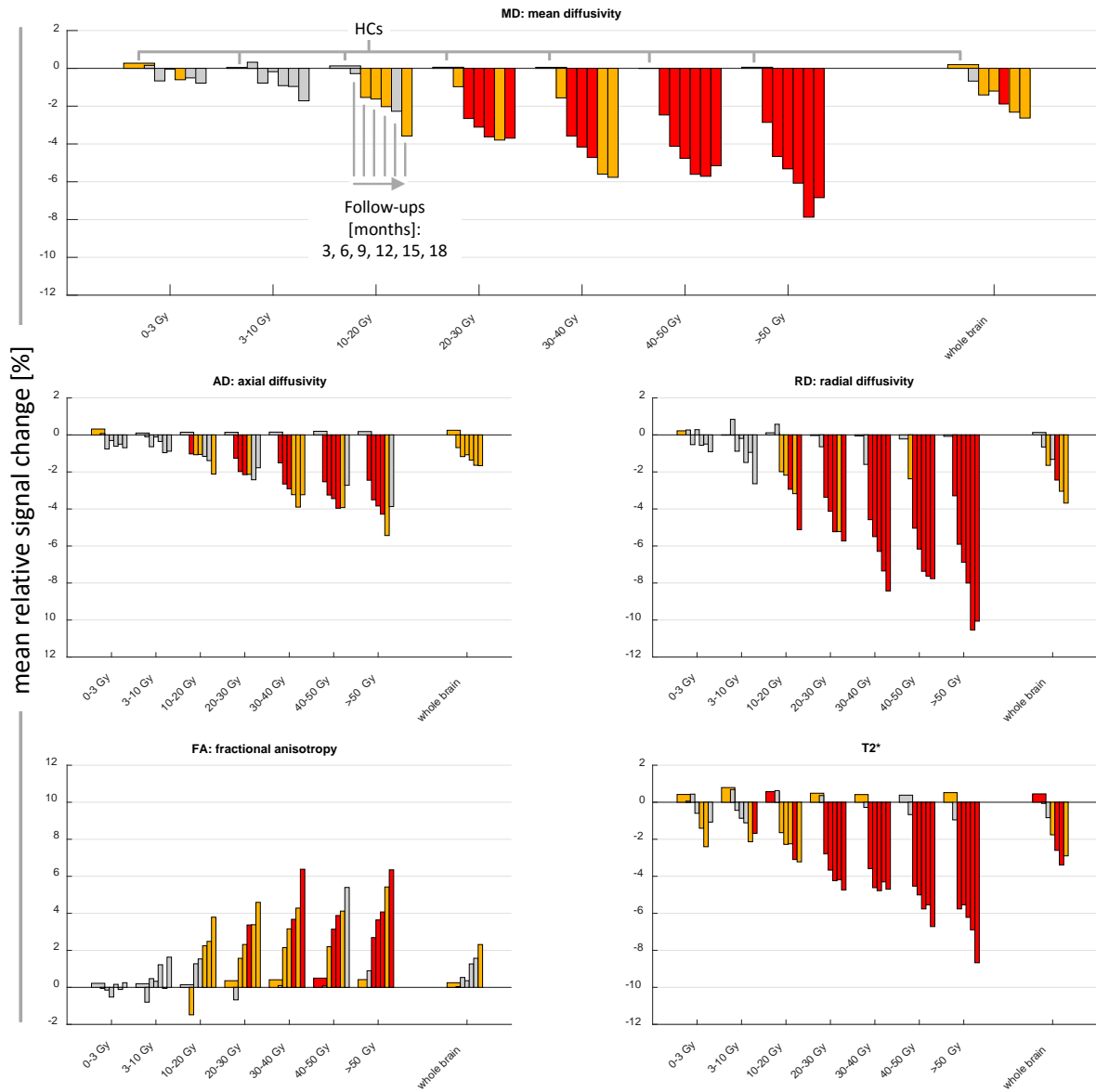


Figure 2: Mean relative signal changes were calculated across all patients and all normal appearing cerebral white matter inside the seven dose bins. Whole brain corresponds to all of the normal appearing cerebral white matter from all dose regions. Mean relative signal changes are plotted for different time points after radio(chemo)therapy (see labels in the MD plot). Mean relative signal changes in the healthy controls (HC) are shown by wider bars. Grey bars indicate no significant signal change, orange bars correspond to  $p < 0.05$  and red bars correspond to a Bonferroni corrected  $p < 0.0042$ . A version of this figure with error bars can be found in the supplementary material (supplementary Figure 6).

5



## Tables

|            | parameter                 | estimate | std.-error | T-stats | significance |
|------------|---------------------------|----------|------------|---------|--------------|
| <b>RD</b>  | b <sub>0</sub> (constant) | 1.75     | 0.73       | 2.40    | 0.026        |
|            | b <sub>1</sub> (dose)     | -0.15    | 0.04       | -3.41   | 0.003        |
|            | b <sub>2</sub> (time)     | -0.18    | 0.03       | -7.09   | <0.001       |
| <b>T2*</b> | b <sub>0</sub> (constant) | 1.15     | 0.97       | 1.19    | 0.250        |
|            | b <sub>1</sub> (dose)     | -0.13    | 0.06       | -1.41   | 0.177        |
|            | b <sub>2</sub> (time)     | -0.08    | 0.04       | -3.26   | 0.002        |

Table 1: Mixed linear models with repeated measurements were used to evaluate the relationship of both radiation dose and time after radiotherapy with the mean relative signal changes of radial diffusivity (RD) and T2\* across whole brain white matter. Estimated parameters for the two mixed linear models  $\Delta S[\%]=b_0+b_1 \times \text{Dose}[\text{Gy}]+b_2 \times \text{Time}[\text{months}]$  for both RD and T2\* are shown. An animation of the fitted RD model is provided as supplementary material.

5

## References

- [1] A. A. Brandes, R. Stupp, P. Hau, D. Lacombe, T. Gorlia, A. Tosoni, R. O. Mirimanoff, J. M. Kros, and M. J. van den Bent. EORTC study 26041-22041: phase I/II study on concomitant and adjuvant temozolomide (TMZ) and radiotherapy (RT) with PTK787/ZK222584 (PTK/ZK) in newly diagnosed glioblastoma. *European journal of cancer (Oxford, England : 1990)*, 46: 348–354 2010. ISSN 1879-0852. doi: [10.1016/j.ejca.2009.10.029](https://doi.org/10.1016/j.ejca.2009.10.029).
- [2] E. L. Chang, S. Akyurek, T. Avalos, N. Rebuena, C. Spicer, J. Garcia, R. Famiglietti, P. K. Allen, K. S. C. Chao, A. Mahajan, S. Y. Woo, and M. H. Maor. Evaluation of peritumoral edema in the delineation of radiotherapy clinical target volumes for glioblastoma. *International journal of radiation oncology, biology, physics*, 68: 144–150 2007. ISSN 0360-3016. doi: [10.1016/j.ijrobp.2006.12.009](https://doi.org/10.1016/j.ijrobp.2006.12.009).
- [3] D. Greene-Schloesser and M. E. Robbins. Radiation-induced cognitive impairment—from bench to bedside. *Neuro-oncology*, 14 Suppl 4: iv37–iv44 2012. ISSN 1523-5866. doi: [10.1093/neuonc/nos196](https://doi.org/10.1093/neuonc/nos196).
- [4] D. B. P. Eekers, E. Roelofs, M. Cubillos-Mesás, C. Niell, R. J. Smeenk, A. Hoeben, A. W. H. Minken, M. Granzier, G. O. Janssens, J. H. A. M. Kaanders, P. Lambin, and E. G. C. Troost. Intensity-modulated proton therapy decreases dose to organs at risk in low-grade glioma patients: results of a multicentric in silico ROCOCO trial. *Acta oncologica (Stockholm, Sweden)*, pages 1–9 2018. ISSN 1651-226X. doi: [10.1080/0284186X.2018.1529424](https://doi.org/10.1080/0284186X.2018.1529424).
- [5] A. Dutz, A. Lühr, L. Agolli, E. G. C. Troost, M. Krause, M. Baumann, X. Vermeren, D. Geismar, E. F. Schapira, M. Bussiére, J. E. Daly, M. R. Bussiére, B. Timmermann, H. A. Shih, and S. Lück. Development and validation of NTCP models for acute side-effects resulting from proton beam therapy of brain tumours. *Radiotherapy and oncology : journal of the European Society for Therapeutic Radiology and Oncology* 2018. ISSN 1879-0887. doi: [10.1016/j.radonc.2018.06.036](https://doi.org/10.1016/j.radonc.2018.06.036).
- [6] J. R. Gunther, M. Sato, M. Chintagumpala, L. Ketonen, J. Y. Jones, P. K. Allen, A. C. Paulino, M. F. Okcu, J. M. Su, J. Weinberg, N. S. Boehling, S. Khatua, A. Adesina, R. Dauser, W. E. Whitehead, and A. Mahajan. Imaging Changes in Pediatric Intracranial Ependymoma Patients Treated With Proton Beam Radiation Therapy Compared to Intensity Modulated Radiation Therapy. *International journal of radiation oncology, biology, physics*, 93: 54–63 2015. ISSN 1879-355X. doi: [10.1016/j.ijrobp.2015.05.018](https://doi.org/10.1016/j.ijrobp.2015.05.018).
- [7] C. R. Peeler, D. Mirkovic, U. Titt, P. Blanchard, J. R. Gunther, A. Mahajan, R. Mohan, and D. R. Grosshans. Clinical evidence of variable proton biological effectiveness in pediatric patients treated

for ependymoma. *Radiotherapy and oncology : journal of the European Society for Therapeutic Radiology and Oncology*, 121: 395–401 2016. ISSN 1879-0887. doi: [10.1016/j.radonc.2016.11.001](https://doi.org/10.1016/j.radonc.2016.11.001).

[8] A. Lühr, C. von Neubeck, M. Krause, and E. G. C. Troost. Relative biological effectiveness in proton beam therapy - Current knowledge and future challenges. *Clinical and translational radiation oncology*, 9: 35–41 2018. ISSN 2405-6308. doi: [10.1016/j.ctro.2018.01.006](https://doi.org/10.1016/j.ctro.2018.01.006).

[9] M. Grech-Sollars, P. W. Hales, K. Miyazaki, F. Raschke, D. Rodriguez, M. Wilson, S. K. Gill, T. Banks, D. E. Saunders, J. D. Clayden, M. N. Gwilliam, T. R. Barrick, P. S. Morgan, N. P. Davies, J. Rossiter, D. P. Auer, R. Grundy, M. O. Leach, F. A. Howe, A. C. Peet, and C. A. Clark. Multi-centre reproducibility of diffusion MRI parameters for clinical sequences in the brain. *NMR in Biomedicine*, 28 (4): 468–485, 2015. ISSN 1099-1492. doi: [10.1002/nbm.3269](https://doi.org/10.1002/nbm.3269). URL <http://dx.doi.org/10.1002/nbm.3269>.

[10] M. Connor, R. Karunamuni, C. McDonald, N. White, N. Pettersson, V. Moiseenko, T. Seibert, D. Marshall, L. Cervino, H. Bartsch, J. Kuperman, V. Murzin, A. Krishnan, N. Farid, A. Dale, and J. Hattangadi-Gluth. Dose-dependent white matter damage after brain radiotherapy. *Radiotherapy and oncology : journal of the European Society for Therapeutic Radiology and Oncology*, 121: 209–216 2016. ISSN 1879-0887. doi: [10.1016/j.radonc.2016.10.003](https://doi.org/10.1016/j.radonc.2016.10.003).

[11] T. R. Hope, J. Vardal, A. Bjørnerud, C. Larsson, M. R. Arnesen, R. A. Salo, and I. R. Groote. Serial diffusion tensor imaging for early detection of radiation-induced injuries to normal-appearing white matter in high-grade glioma patients. *J Magn Reson Imaging*, 41 (2): 414–423 2015. doi: [10.1002/jmri.24533](https://doi.org/10.1002/jmri.24533). URL <http://dx.doi.org/10.1002/jmri.24533>.

[12] V. Nagesh, C. I. Tsien, T. L. Chenevert, B. D. Ross, T. S. Lawrence, L. Junick, and Y. Cao. Radiation-induced changes in normal-appearing white matter in patients with cerebral tumors: a diffusion tensor imaging study. *Int J Radiat Oncol Biol Phys*, 70 (4): 1002–1010 2008. doi: [10.1016/j.ijrobp.2007.08.020](https://doi.org/10.1016/j.ijrobp.2007.08.020). URL <http://dx.doi.org/10.1016/j.ijrobp.2007.08.020>.

[13] C. H. Chapman, T. Zhu, M. Nazem-Zadeh, Y. Tao, H. A. Buchtel, C. I. Tsien, T. S. Lawrence, and Y. Cao. Diffusion tensor imaging predicts cognitive function change following partial brain radiotherapy for low-grade and benign tumors. *Radiotherapy and oncology : journal of the European Society for Therapeutic Radiology and Oncology*, 120: 234–240 2016. ISSN 1879-0887. doi: [10.1016/j.radonc.2016.06.021](https://doi.org/10.1016/j.radonc.2016.06.021).

[14] C. H. Chapman, M. Nazem-Zadeh, O. E. Lee, M. J. Schipper, C. I. Tsien, T. S. Lawrence, and Y. Cao. Regional variation in brain white matter diffusion index changes following

- chemoradiotherapy: a prospective study using tract-based spatial statistics. *PLoS one*, 8: e57768, 2013. ISSN 1932-6203. doi: [10.1371/journal.pone.0057768](https://doi.org/10.1371/journal.pone.0057768).
- [15] M.-R. Nazem-Zadeh, C. H. Chapman, T. L. Lawrence, C. I. Tsien, and Y. Cao. Radiation therapy effects on white matter fiber tracts of the limbic circuit. *Medical physics*, 39: 5603–5613 2012. ISSN 0094-2405. doi: [10.1118/1.4745560](https://doi.org/10.1118/1.4745560).
- [16] C. H. Chapman, V. Nagesh, P. C. Sundgren, H. Buchtel, T. L. Chenevert, L. Junck, T. S. Lawrence, C. I. Tsien, and Y. Cao. Diffusion tensor imaging of normal-appearing white matter as biomarker for radiation-induced late delayed cognitive decline. *International journal of radiation oncology, biology, physics*, 82: 2033–2040 2012. ISSN 1879-355X. doi: [10.1016/j.ijrobp.2011.01.068](https://doi.org/10.1016/j.ijrobp.2011.01.068).
- 10 [17] M. Connor, R. Karunamuni, C. McDonald, T. Seibert, N. White, V. Moiseenko, H. Bartsch, N. Farid, J. Kuperman, A. Krishnan, A. Dale, and J. A. Hattangadi-Gluth. Regional susceptibility to dose-dependent white matter damage after brain radiotherapy. *Radiotherapy and oncology : journal of the European Society for Therapeutic Radiology and Oncology*, 123: 209–217 2017. ISSN 1879-0887. doi: [10.1016/j.radonc.2017.04.006](https://doi.org/10.1016/j.radonc.2017.04.006).
- 15 [18] T. Zhu, C. H. Chapman, C. Tsien, M. Kim, D. E. Spratt, T. S. Lawrence, and Y. Cao. Effect of the Maximum Dose on White Matter Fiber Bundles Using Longitudinal Diffusion Tensor Imaging. *International journal of radiation oncology, biology, physics*, 96: 696–705 2016. ISSN 1879-355X. doi: [10.1016/j.ijrobp.2016.07.010](https://doi.org/10.1016/j.ijrobp.2016.07.010).
- [19] M. Makola, M. Douglas Ris, E. M. Mahone, K. O. Yeates, and K. M. Cecil. Long-term effects of radiation therapy on white matter of the corpus callosum: a diffusion tensor imaging study in children. *Pediatric radiology*, 47: 1809–1816 2017. ISSN 1432-1998. doi: [10.1007/s00247-017-3955-1](https://doi.org/10.1007/s00247-017-3955-1).
- 20 [20] S. Wang, E. X. Wu, D. Qiu, L. H. T. Leung, H.-F. Lau, and P.-L. Khong. Longitudinal diffusion tensor magnetic resonance imaging study of radiation-induced white matter damage in a rat model. *Cancer research*, 69: 1190–1198 2009. ISSN 1538-7445. doi: [10.1158/0008-5472.CAN-08-2661](https://doi.org/10.1158/0008-5472.CAN-08-2661).
- 25 [21] I. O. Jelescu, M. Zurek, K. V. Winters, J. Veraart, A. Rajaratnam, N. S. Kim, J. S. Babb, T. M. Shepherd, D. S. Novikov, S. G. Kim, and E. Fieremans. In vivo quantification of demyelination and recovery using compartment-specific diffusion MRI metrics validated by electron microscopy. *NeuroImage*, 132: 104–114 2016. ISSN 1095-9572. doi: [10.1016/j.neuroimage.2016.02.004](https://doi.org/10.1016/j.neuroimage.2016.02.004).
- [22] K. D. Harkins, J. Xu, A. N. Dula, K. Li, W. M. Valentine, D. F. Gochberg, J. C. Gore, and M. D. Does. The microstructural correlates of T1 in white matter. *Magnetic resonance in medicine*, 75: 1341–1345 2016. ISSN 1522-2594. doi: [10.1002/mrm.25709](https://doi.org/10.1002/mrm.25709).
- 30

- [23] C. H. Cunningham, J. M. Pauly, and K. S. Nayak. Saturated double-angle method for rapid B1+ mapping. *Magn Reson Med*, 55 (6): 1326–1333 2006. doi: [10.1002/mrm.20896](https://doi.org/10.1002/mrm.20896). URL <http://dx.doi.org/10.1002/mrm.20896>.
- [24] J. L. R. Andersson, S. Skare, and J. Ashburner. How to correct susceptibility distortions in spin-echo echo-planar images: application to diffusion tensor imaging. *Neuroimage*, 20 (2): 870–888 2003. doi: [10.1016/S1053-8119\(03\)00336-7](https://doi.org/10.1016/S1053-8119(03)00336-7). URL [http://dx.doi.org/10.1016/S1053-8119\(03\)00336-7](http://dx.doi.org/10.1016/S1053-8119(03)00336-7).
- [25] S. M. Smith, M. Jenkinson, M. W. Woolrich, C. F. Beckmann, T. E. J. Behrens, H. Johansen-Berg, P. R. Bannister, M. De Luca, I. Drobnjak, D. E. Flitney, R. K. Niazy, J. Saunders, J. Vickers, Y. Zhang, N. De Stefano, J. M. Brady, and P. M. Matthews. Advances in functional and structural MR image analysis and implementation as FSL. *NeuroImage*, 23 Suppl 1: S208–S219, 2004. ISSN 1053-8119. doi: [10.1016/j.neuroimage.2004.07.051](https://doi.org/10.1016/j.neuroimage.2004.07.051).
- [26] A. Peña, H. A. L. Green, T. A. Carpenter, S. J. Price, J. D. Pickard, and J. H. Gillard. Enhanced visualization and quantification of magnetic resonance diffusion tensor imaging using the p:q tensor decomposition. *Br J Radiol*, 79 (938): 101–109 2006. doi: [10.1259/bjr/24908512](https://doi.org/10.1259/bjr/24908512). URL <http://dx.doi.org/10.1259/bjr/24908512>.
- [27] B. B. Avants, N. J. Tustison, G. Song, P. A. Cook, A. Klein, and J. C. Gee. A reproducible evaluation of ANTs similarity metric performance in brain image registration. *NeuroImage*, 54: 2033–2044 2011. ISSN 1095-9572. doi: [10.1016/j.neuroimage.2010.09.025](https://doi.org/10.1016/j.neuroimage.2010.09.025).
- [28] N. J. Tustison and B. B. Avants. Explicit B-spline regularization in diffeomorphic image registration. *Frontiers in neuroinformatics*, 7: 39, 2013. ISSN 1662-5196. doi: [10.3389/fninf.2013.00039](https://doi.org/10.3389/fninf.2013.00039).
- [29] J. Lee, K. Shmueli, B.-T. Kang, B. Yao, M. Fukunaga, P. van Gelderen, S. Palumbo, F. Bosetti, A. C. Silva, and J. H. Duyn. The contribution of myelin to magnetic susceptibility-weighted contrasts in high-field MRI of the brain. *NeuroImage*, 59: 3967–3975 2012. ISSN 1095-9572. doi: [10.1016/j.neuroimage.2011.10.076](https://doi.org/10.1016/j.neuroimage.2011.10.076).
- [30] S. H. Fung, L. Roccatagliata, R. G. Gonzalez, and P. W. Schaefer. MR diffusion imaging in ischemic stroke. *Neuroimaging clinics of North America*, 21: 345–77, xi 2011. ISSN 1557-9867. doi: [10.1016/j.nic.2011.03.001](https://doi.org/10.1016/j.nic.2011.03.001).
- [31] M. D. Budde, L. Janes, E. Gold, L. C. Turtzo, and J. A. Frank. The contribution of gliosis to diffusion tensor anisotropy and tractography following traumatic brain injury: validation in the rat

using Fourier analysis of stained tissue sections. *Brain : a journal of neurology*, 134: 2248–2260 2011. ISSN 1460-2156. doi: [10.1093/brain/awr161](https://doi.org/10.1093/brain/awr161).

[32] S. Saxena and P. Caroni. Mechanisms of axon degeneration: from development to disease. *Progress in neurobiology*, 83: 174–191 2007. ISSN 0301-0082. doi: [10.1016/j.pneurobio.2007.07.007](https://doi.org/10.1016/j.pneurobio.2007.07.007).

5 [33] C. A. Colton. Heterogeneity of microglial activation in the innate immune response in the brain. *Journal of neuroimmune pharmacology : the official journal of the Society on NeuroImmune Pharmacology*, 4: 399–418 2009. ISSN 1557-1904. doi: [10.1007/s11481-009-9164-4](https://doi.org/10.1007/s11481-009-9164-4).

[34] M. Hermier, N. Nighoghossian, L. Derex, M. Wiart, C. Nemoz, Y. BerthezÃ¨ne, and J. C. Froment. Hypointense leptomeningeal vessels at T2\*-weighted MRI in acute ischemic stroke.  
10 *Neurology*, 65: 652–653 2005. ISSN 1526-632X. doi: [10.1212/01.wnl.0000173036.95976.46](https://doi.org/10.1212/01.wnl.0000173036.95976.46).

[35] J. Petr, I. Platzek, A. Seidlitz, H. J. M. M. Mutsaerts, F. Hofheinz, G. Schramm, J. Maus, B. Beuthien-Baumann, M. Krause, and J. van den Hoff. Early and late effects of radiochemotherapy on cerebral blood flow in glioblastoma patients measured with non-invasive perfusion MRI. *Radiother Oncol*, 118 (1): 24–28 2016. doi: [10.1016/j.radonc.2015.12.017](https://doi.org/10.1016/j.radonc.2015.12.017). URL <http://dx.doi.org/10.1016/j.radonc.2015.12.017>.  
15

[36] M. Quarantelli. MRI/MRS in neuroinflammation: methodology and applications. *Clinical and translational imaging*, 3: 475–489, 2015. ISSN 2281-5872. doi: [10.1007/s40336-015-0142-y](https://doi.org/10.1007/s40336-015-0142-y).